# Study of the Decay Parameters and Magnetic Moment of the $\Xi^-$†

G. McD. Bingham,* V. Cook, J. W. Humphrey,‡ O. R. Sander,§ and R. W. Williams
*Department of Physics, University of Washington, Seattle, Washington 98105*

and

G. E. Masek, T. Maung, and H. Ruderman
*Department of Physics, University of California, San Diego, La Jolla, California 92037*

(Received 29 January 1970)

This paper describes an experimental study of the decay parameters and the magnetic moment of the $\Xi^-$. A 1.8-GeV/$c$ $K^-$ beam derived from the Bevatron was used to produce $\Xi^-$ by the reaction $K^-p \to \Xi^-K^+$. The $K^+$ and resulting decay products of the $\Xi^-$ were used to trigger a spark-chamber system, pictures from which yielded a total of 2724 events which passed all measuring criteria. The $\Xi^-$ were produced in an intense (170 kG) magnetic field obtained from a pulsed magnet. The precession of the magnetic moment of the $\Xi^-$ in the presence of this field can be measured from the angular distribution of the $\Xi^-$ decay products and a value of the magnetic moment obtained. The decay parameters and polarization of the $\Xi^-$ are also obtained from the angular distribution of the decay products; we obtain $\alpha = -0.383 \pm 0.065$, $\Phi = -(26 \pm 30)°$, and $\bar{P} = 0.19 \pm 0.09$. The accuracy of the magnetic moment value is severely limited by the low value of polarization and experimental biases in the distribution; we obtain $\mu_{\Xi^-} = -0.1 \pm 2.1$ nuclear magnetons.

## I. INTRODUCTION

ALTHOUGH most of the information now available on the $\Xi^-$ (cascade) particle comes from bubble chambers, the $\Xi^-$ is well suited to spark-chamber studies: It has a characteristic signature in production and decay. Experience with a spark-chamber measurement of the magnetic moment[1] of the $\Sigma^+$ led us to attempt a similar measurement on the $\Xi^-$, using a refined version of the pulsed-magnet method of the former work. This paper describes the results of a study of $\Xi^-$'s produced at the Bevatron by 1.8-GeV/$c$ $K^-$ mesons, precessed in a pulsed magnet, and detected in optical spark chambers. A new determination of the decay parameter $\alpha$ is reported, along with estimates of the other decay parameters and the magnetic moment. The latter depend on the polarization of the sample, which proved to be less than the available bubble-chamber data[2] had suggested.

The reaction $K^-p \to \Xi^-K^+$ yields a $\Xi^-$ predominantly forward at 1.8-GeV/$c$ $K^-$ momentum; the experimental arrangement allowed the $\Xi^-$ to pass through a solenoid centered on the beamline and decay into the (nearly) axially symmetric detection apparatus. The trigger demanded a particle at $\sim 90°$ (the $K^+$), a single forward-going particle with velocity less than $0.85c$ (the $\Xi^-$), and three charged particles in the final state downstream (two $\pi^-$'s and the proton). The $\Xi^-$ momentum was parallel, or antiparallel, to a magnetic field of up to 180 kG.

The decay parameter $\alpha$ was found to be $\alpha = -0.383 \pm 0.065$, and the value of $\Phi = -(26 \pm 30)°$, where $\sin\Phi = \beta/(1-\alpha^2)^{1/2}$, $\cos\Phi = \gamma/(1-\alpha^2)^{1/2}$. The mean value of the polarization of the sample chosen was $\bar{P} = 0.19 \pm 0.09$. From the rotation of the polarization, the magnetic moment determination gave $\mu = -0.1 \pm 2.1$ $\mu_N$. The definition of the decay parameters $\alpha$, $\beta$, and $\gamma$ is that used in the Particle Data Group compilation.[3]

## II. EXPERIMENTAL APPARATUS

The general arrangement of the experimental setup is shown in Fig. 1, and the details of the detector region are shown in Fig. 2. $K^-$ mesons of momentum 1.8 GeV/$c$, produced on a Bevatron internal target, were separated and directed onto a 4-in. polyethylene target placed in the bore of a pulsed magnet (bore 9.4 cm in diameter and 13 cm long—maximum field $\sim 180$ kG). The reaction $K^-p \to \Xi^-K^+$ was used to produce the $\Xi^-$. The incident $K^-$, the $\Xi^-$, and the charged decay products resulting from $\Xi^- \to \pi^-\Lambda^0 \to \pi^-\pi^-p$ were observed in spark chambers SC1–SC5. The chambers were triggered by requiring that (1) a particle be seen at near 90° to the production target in the $K$ counters, (2) a particle have a velocity less than $0.85c$ in the Čerenkov counter C2 and less than twice minimum ionizing in the $dE/dx$ counter AP YES (this requirement is compatible with a single $\Xi^-$ emerging from the bore of the magnet), and finally, (3) three charged particles be seen downstream of SC5 in the counters S1–S12 and L1–L6 and one of these particles be close to the beam axis. Thus the com-

† Supported by the National Science Foundation.

* Present address: National Accelerator Laboratory, Batavia, Ill.

‡ Present address: Istituto Nazionale di Fisica Nucleare, Via G. Marconi 10, Naples, Italy.

§ Present address: Physics Department, University of Notre Dame, Notre Dame, Ind.

[1] V. Cook, T. Ewart, G. Masek, R. Orr, and E. Platner, Phys. Rev. Letters **17**, 223 (1966).

[2] D. D. Carmony, G. M. Pjerrou, P. E. Schlein, W. E. Slater, D. H. Stork, and H. K. Ticho, Phys. Rev. Letters **12**, 482 (1964); J. P. Berge, P. Eberhard, J. R. Hubbard, D. W. Merrill, J. Button-Shafer, F. T. Solmitz, and M. L. Stevenson, Phys. Rev. **147**, 945 (1966); J. Button-Shafer, J. Berge, and P. Schlein (private communications).

[3] N. Barash-Schmidt, A. Barbaro-Galtieri, L. R. Price, A. H. Rosenfeld, P. Söding, C. G. Wohl, M. Roos, and G. Conforto, Rev. Mod. Phys. **41**, 109 (1969).

plete trigger was

$$(B2)(C1)(B3)(K)(C2)(AP\ YES)(AP\ ANTI)[(S1\text{–}S12, L1\text{–}L6)\geq 3][(S1\text{–}S12)\geq 1].$$

### A. Beam

From the bubble-chamber data available to us, it appeared that 1.8 GeV/$c$ was the optimum momentum for the $K^-$ beam: The kinematics were favorable, the cross section was peaked for forward $\Xi^-$, totaling 90 $\mu$b in the angular region accepted, and the polarization seemed greater than 0.5, though with poor statistics. Calculation showed that the UCRL Bevatron, with $3\times10^{12}$ protons per pulse at 7 GeV/$c$, could furnish a $K^-$ flux of approximately 10 000 per pulse, provided a beam with good separation, a large momentum window, and reasonably short total length could be built. These criteria were met by a somewhat unconventional design in which only one intermediate focus was used, a highly astigmatic double focus. The dispersed horizontal focus occurred 2.3 m upstream from the vertical focus and mass slit. A rather strong sextupole field at the horizontal focus afforded compensation of the chromatic aberration at the mass slit. The general layout is shown in Fig. 1. The beam was taken at 0° from an internal target, and the dispersion was provided by the Bevatron fringing field. Some characteristics of the beam are given in Table I. Note that the separation factor was quite good despite the large momentum window. Further details on the beam can be found in the dissertation of Sander.[4]

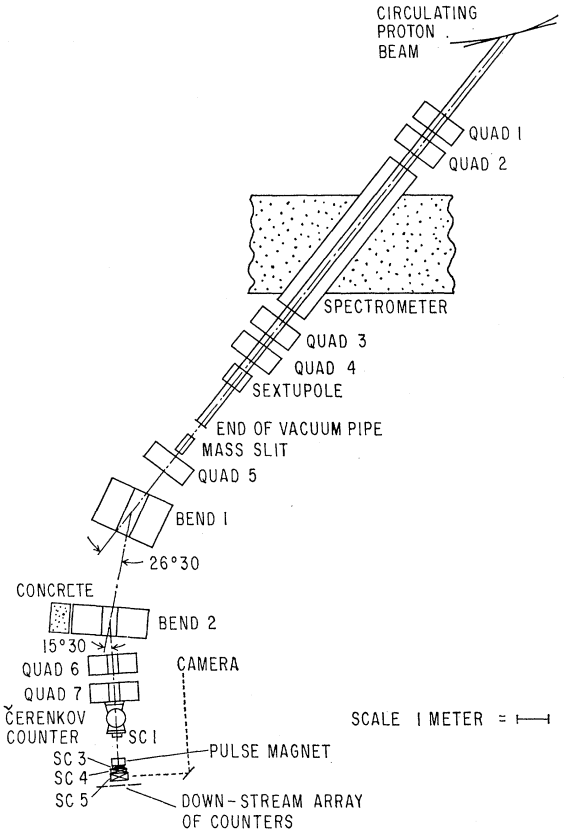


FIG. 1. Layout of 1.8-GeV/$c$ $K^-$ beam used in the experiment. See text and Table I for a description of the beam. The final focus is located at the pulsed magnet. Also shown is the general arrangement of the detectors and the optical system.

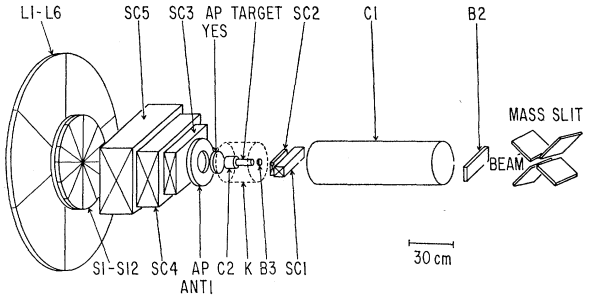


FIG. 2. Experimental arrangement for producing and detecting $\Xi^-$. The $\Xi^-$ are produced in the reactions $K^-+p\rightarrow\Xi^-+K^+$. The $K^+$ and decay products from $\Xi^-\rightarrow\Lambda^0+\pi^-$ and $\Lambda^0\rightarrow p+\pi^-$ are used to trigger the spark chambers, as described in the text. The target is 4 in. of polyethylene and together with C2, K, and B3 is located in the bore of the pulsed magnet. C1 is a gas Čerenkov counter used to separate $K^-$ from $\pi^-$ to electronically. All other components are defined in the text. The logic for triggering the spark chambers was (B2)(C1)(B3)(K)(C2)(AP YES)(AP ANTI) $[(S1\text{–}S12, L1\text{–}L6)\geq 3][(S1\text{–}S12)\geq 1]$.

The $\pi/K$ ratio at the $\Xi^-$ production target was 4/1; $K$'s were selected and pions rejected by a 30-cm-bore differential Čerenkov counter specially designed for this beam. The effective pion contamination was reduced by this selection to 4%.

TABLE I. Properties of the separated $K^-$-meson beam.

| | |
|---|---|
| Internal target | $\frac{1}{16}\times\frac{1}{4}\times4$ in. |
| Internal target material | Copper |
| Length of beam | 1070 in. or 2.06 $K^-$ decay lengths |
| Momentum | 1.8 BeV/$c$ |
| Momentum bite | ±3% |
| Acceptance | 4.18 msr % |
| $K^-$-meson yield on 1.37-in. defining counter, with $3\times10^{12}$ protons on target | 9000 |
| $K^-$-meson yield on 6-in. counter | 10 500 |
| $\pi/K^-$-meson ratio on 1.37-in. counter | 3.9 |
| $\pi/K^-$-meson ratio on 6-in. counter | 6.3 |
| Vertical size of beam at the mass slit | 0.06 in. |
| Diameter of final focus | 0.9 in. |
| $\pi^-$-meson contamination of $K^-$ mesons | 4% |
| Separation image | 2 |
| $\pi^-/K^-$-meson ratio using peak transmission rates | 600 |
| $\pi^-$-meson rejection factor due to the mass slit | 150 |
| Average slit transmission | 83% |

[4] O. R. Sander, thesis, University of Washington, 1969 (unpublished).

### B. Experimental Arrangement and Detection

The high-momentum forward-going $\Xi^-$'s had a mean path for decay of around 7 cm. The physical length of the solenoid magnet could not be made less than 20 cm without sacrificing either field or acceptance solid angle. The polyethylene target for the $\Xi^-$ production was therefore placed inside the solenoid, permitting the observation, in a downstream spark chamber, of both the $\Xi^-$ decay and the subsequent $\Lambda$ decay. The $K^+$, which typically leaves the target at $\sim 90°$, thus could not escape from the magnet. Its presence, with a coarse indication of its direction, was signaled by one of four counters, each covering 90° of azimuth.[5] Figure 2 shows an exploded view of the experimental arrangement. The four azimuthal counters are indicated by the dashed line labeled K.

The rest of the trigger logic demanded that the $\Xi^-$ be an unaccompanied particle with velocity less than $0.85c$, and that there be exactly three charged particles downstream, of which at least one was near the beam axis. The latter criterion, suggested by the kinematics of $\Xi^- \to \pi^- + \Lambda$, $\Lambda \to \pi^- + p$, was studied by Monte Carlo methods, and a wheel of counters was designed on the basis of this study. In Fig. 2 the 12 inner counters and six outer counters can be seen at the left (S1–S12 and L1–L6). The tests on the $\Xi^-$, which was expected to have a $\beta \approx 0.8$, were made by a small threshold Čerenkov counter (C2), of fluorochemical FC75, which rejected relativistic pions with 95% efficiency, and a $dE/dx$ scintillation counter AP YES, which required that one particle be present but gave a veto if the pulse height was as large as that of two minimum-ionizing particles.

The trigger criteria were effective in responding to $\Xi^-$ events while reducing[6] the rate from the far more copious products of $K^-p$ and $K^-n$ interactions. However, the requirements imposed on the decay products caused some correlations in the data. These were studied by Monte Carlo methods and are treated in Sec. IV.

In Fig. 2 the optical spark chambers which provided the data of the experiment are labeled SC1–SC5. The instantaneous rates in these chambers were high (the Bevatron beam pulse was matched to the duration of the magnet pulse); the two in-beam chambers were supplemented by a counter hodoscope (not shown) which selected the correct incident $K^-$ track if more than one track occurred in the spark chambers. Photographs were taken with a specially constructed four-lens camera with fast shutters. This camera took up to four pictures per pulse on 30×70 mm format, with 10 msec dead time between pictures.

Figure 3 is an example of a $\Xi^-$ decay event.

[5] A more complex $K^+$ detector, including a cylindrical spark chamber coaxial with the target, was tried but was not successful. There was inconclusive evidence that spark formation was inhibited by the strong transverse magnetic field.

[6] J. W. Humphrey, thesis, University of Washington, 1969 (unpublished).

### C. Magnet

The pulsed magnet system was an improved version of the system used in the $\Sigma^+$ magnetic moment experiment.[1] It provided a usable volume 9.4 cm diam×13 cm long, a peak field of 170 kG for most of the experiment and 180 kG in the last phase, and a pulse length of 60 msec full width at half-maximum (FWHM). In addition, this magnet was extremely reliable. At the end of the experiment, after $2.6\times10^5$ pulses, it showed no evidence of deterioration.

Figure 4 shows a drawing of the magnet. It is a single flat helix of 22 turns, inner diameter 10.4 cm, outer diameter 24.8 cm, cut from a single billet of heat-treated high-conductivity chrome copper (0.8% chromium). A hardened-steel shell and end plates contained the coil, which was insulated with melamine-formaldehyde-impregnated fiberglass. Cooling was by axial water flow along the inside and outside surfaces of the coil, at 65 gal/min.

The long duration of magnetic field was obtained, despite the low inductance of the coil (36 $\mu$H), by discharging a high-$C$ low-voltage bank of electrolytic capacitors through the coil. The 10 000 capacitors had a total capacitance of 17 F and operated at 310 V. Diodes across the capacitors carried the current during the reversed-voltage portion of the pulse, so that the entire stored energy, 0.8 MJ, was deposited in the magnet. The repetition period used was 11 sec, corresponding to every second Bevatron pulse.

Figure 5 shows the time variation and space variation (along the axis) of the field. The entire field was carefully mapped, and the integral of field along the path was numerically computed for each $\Xi^-$. The origin of each path in the target was determined from the intersection of the fitted $\Xi^-$ and $K^-$ direction. The instantaneous value of the field for each event was obtained by recording, within one msec of the trigger signal, the integrated voltage from a pickup coil permanently mounted in the bore of the magnet. A digital display of this voltage appeared on the frame in which the event was photographed. The over-all accuracy of the magnetic field determination was 4%.

## III. SELECTION, MEASUREMENT, AND FITTING OF EVENTS

A preliminary run, with no magnet and with "auxiliary spark chambers" to measure the $K^+$ direction, was scanned for $\Xi^-$ events and measured on projection microscopes. From the asymmetry observed in the correlation between the $\Lambda$ momentum and the production plane normal, we found the $\Xi^-$ polarization $P = +0.55 \pm 0.29$. A later, more refined analysis reduced this to $+0.32 \pm 0.24$. The sign and magnitude were consistent with the (fragmentary) bubble-chamber data, and the decision was made to accept 1.8 GeV/$c$ as the operating beam momentum. As is shown below, the final sample polarization was lower.

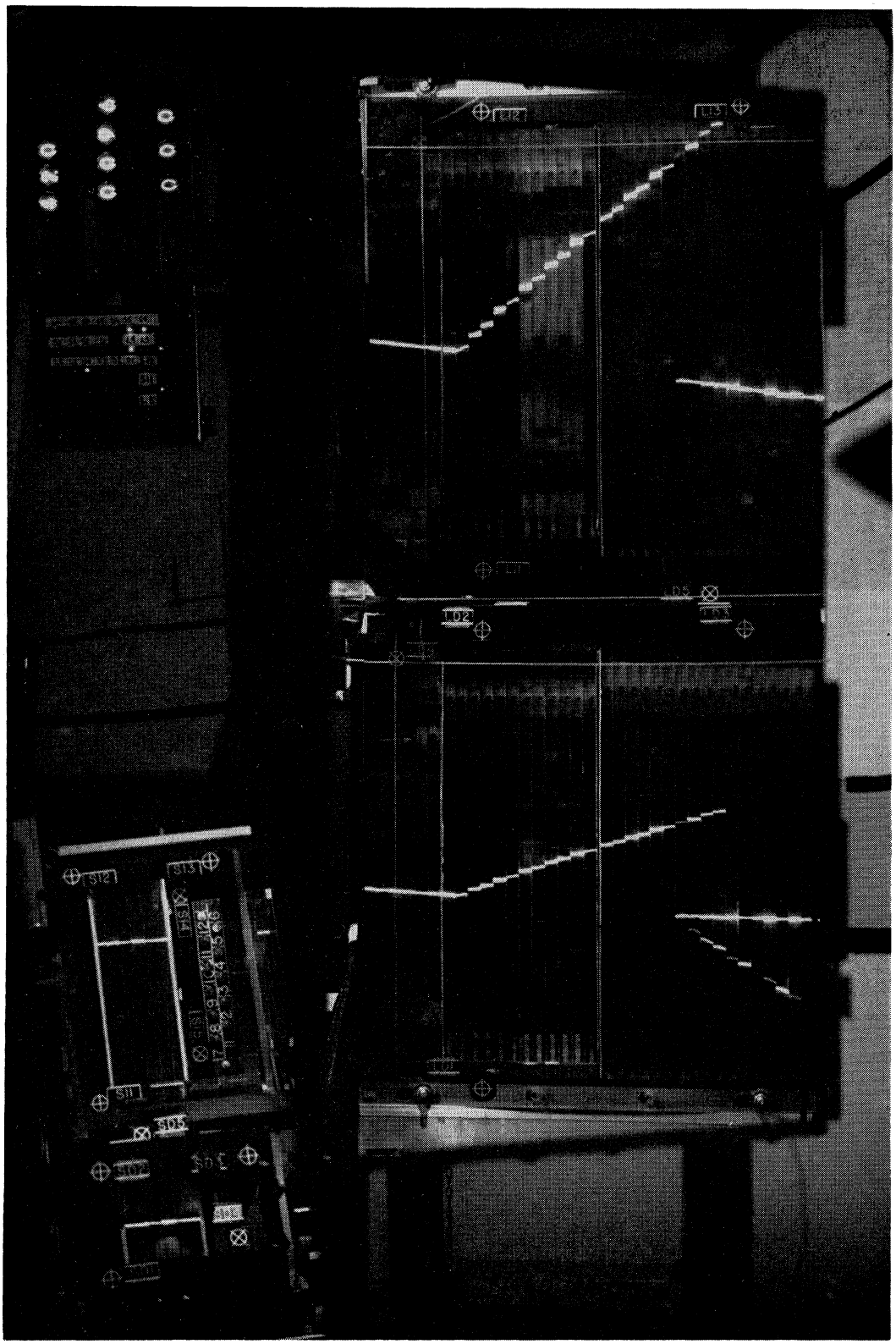

FIG. 3. Example of cascade decay event seen in spark chambers SC3, SC4, and SC5. Cascade enters from left and decays into $\pi^-$ and $\Lambda^0$. Subsequent decay of $\Lambda^0$ into $p+\pi^-$ is seen in far right of chambers.

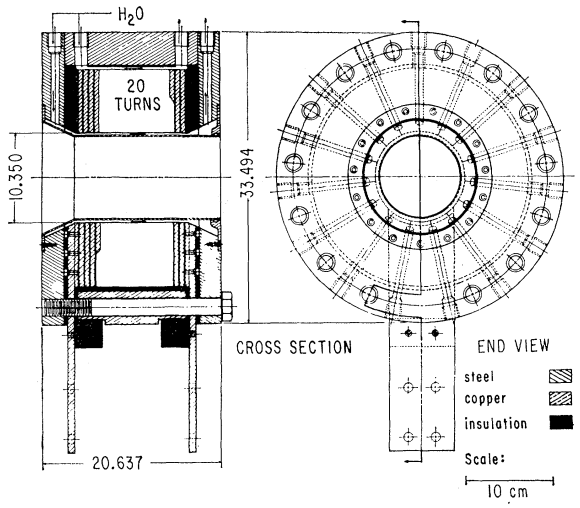


FIG. 4. Drawing of pulsed magnet.

During the actual running, data were taken with both directions of the magnetic field, and with zero field. A total of $5\times10^5$ pictures was obtained. From this sample, 4564 pictures were found which appeared to contain a $\Xi^-$ decay and a subsequent $\Lambda$ decay. The events were reconstructed by MUXIA, a CDC 6600 program written by one of us (HR). Using the slopes and intercepts of the measured spark chamber tracks, MUXIA reconstructed each event in four steps:

(1) MUXIA first fitted the tracks of the $\Xi^-$ and the tracks of the charged decay particles of the $\Xi^-$ and $\Lambda$, subject to the constraints imposed by copunctuality and coplanarity. This portion of the program employed the techniques of the UCRL fitting program GUTS. A $\chi^2$ for the fit was calculated. If the fit converged to a $\chi^2$ less than 100 (four degrees of freedom), MUXIA proceeded to step 2. Otherwise MUXIA rejected the event.

(2) The kinematics of the $\Xi^-$ decay were examined and appropriate kinematical variables were fitted. If the fit converged, MUXIA proceeded to step 3. (In this and the following steps, a fitting procedure similar to that used by the CERN fitting program GRIND was employed.)

(3) Using the $\Xi^-$ momentum calculated in step 2, the $\Xi^-$ production kinematics were examined, and appropriated variables were fitted assuming the target particle was a free proton. The fitting program provided the momenta $\mathbf{K}$, $\mathbf{\Xi}$, $\mathbf{\Lambda}$, $\mathbf{p}$, and the integral $\int\mathbf{B}\cdot d\mathbf{l}$ along the path of the $\Xi^-$ for $\Xi^-$'s which satisfied reasonable production kinematics and therefore were largely produced on free or quasifree protons.

(4) The kinematics of the entire event were examined, and the kinematical variables were adjusted for best fit.

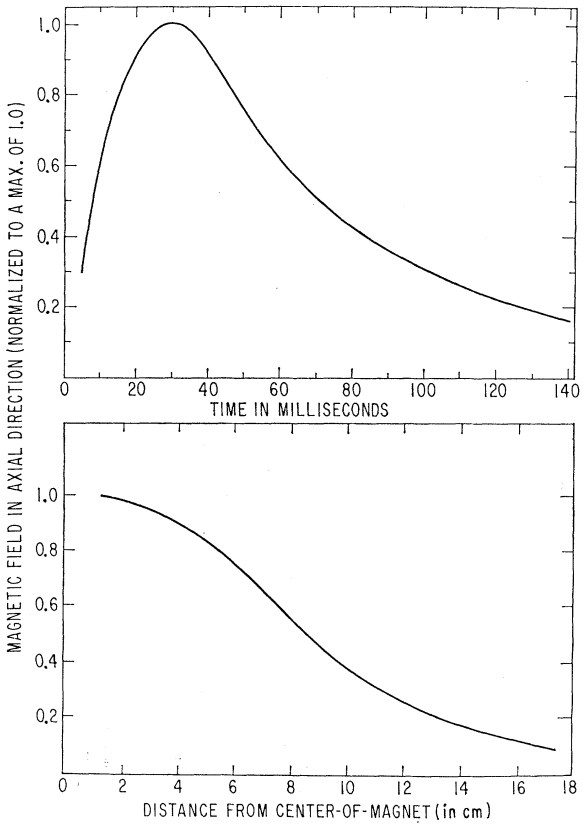


FIG. 5. Time and space variation (along the axis) of axial component of magnetic field in the pulsed magnet. The peak field was 170 kG for most of the experiment.

The reason for this series of fits is computing efficiency. The procedure outlined above allowed MUXIA to calculate an initial guess that was reasonably close to the final result. Convergence at each step was obtained after about four or five iterations.

Of the 4564 events that satisfied our scanning criteria, 3381 survived our fitting program. The fitting program did not include the fact that we knew which $K$ counter the $K^+$ triggered. When we demanded that the calculated azimuthal intersection of the $K^+$ trajectory with the ring of $K$ counters be within 60° of the center of the triggering counter, and made a c.m. angle cut, we were left with a sample of 2724 events which had a c.m. angle between 10° and 80°. Restricting the c.m. angle to (20–80)° was found to improve the polarization. After this cut, the sample consisted of 2433 events, as follows: field downstream, 690; field upstream, 786; zero field, 957.

The number of candidate events found agrees with our calculations using the bubble-chamber cross sections.[2] The rejection rate is also reasonable since the calculations indicate that somewhat more than half the events are either $\Xi^-$ from carbon or $\Xi^{*-}$ from carbon or hydrogen.

## IV. ANALYSIS AND RESULTS

### A. Decay Distributions and Biases

The joint distribution function for the two-stage decay of a $\Xi^-$ with polarization $P\hat{N}$ has the form

$$(4\pi)^2 I(\hat{N},\hat{\Lambda},\hat{p}) = 1+\alpha_\Lambda \hat{p}\cdot\hat{\Lambda}+P\{\alpha\hat{\Lambda}\cdot\hat{N}+\alpha_\Lambda\hat{p}\cdot[(\hat{\Lambda}\cdot\hat{N})\hat{\Lambda} +\beta\hat{N}\times\hat{\Lambda}+\gamma\hat{\Lambda}\times(\hat{N}\times\hat{\Lambda})]\}. \quad (1)$$

The directions are defined in Fig. 6. The presence of a magnetic field causes the polarization direction at decay to be shifted from the production normal $\hat{N}_0=(\hat{K}^-\times\hat{\Xi}^-)/|\hat{K}^-\times\hat{\Xi}^-|$. For our experimental conditions with $\hat{\Xi}^-$ nearly parallel to the magnetic field, the effect is to precess the spin direction about $\hat{\Xi}^-$ as an axis through an angle proportional to the $\Xi^-$ magnetic moment and to the integral of the field along the trajectory.

The distribution of detected $\Xi^-$'s differs from Eq. (1) because of biases introduced by the experimental apparatus. These biases can be represented by multiplying the decay distribution by an efficiency function $E(\hat{N},\hat{\Lambda},\hat{p})$. A rather elaborate Monte Carlo model of the experiment was studied to discover sources of biases and to compute the efficiency function.[6]

To simplify the analysis, we chose to look at projections of the distribution function. In particular, consider the distributions

$$4\pi I_{\Lambda N}(\cos\theta)d\Omega=[1+\alpha P\hat{\Lambda}\cdot\hat{N}]d\Omega \quad (2)$$

and

$$4\pi I_{pN}(\cos\theta')d\Omega=[1+\alpha_\Lambda(\tfrac{2}{3}\gamma+\tfrac{1}{3})P\hat{p}\cdot\hat{N}]d\Omega, \quad (3)$$

where $\alpha_\Lambda$ is the $\Lambda$-particle decay parameter, $\cos\theta=\hat{\Lambda}\cdot\hat{N}$ and $\cos\theta'=\hat{p}\cdot\hat{N}$, and $I(\cos\theta)d\Omega$ is the probability that one vector lies in $d\Omega$ at polar angle $\theta$ from the other. Equation (2) is the familiar $\Xi^-$ decay asymmetry, while Eq. (3) contains information from the $\Lambda$ decay about the magnitude and direction of the $\Xi^-$ polarization.[7]

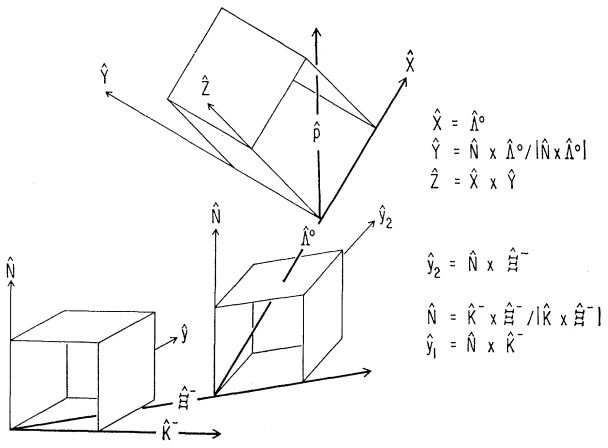


FIG. 6. Definition of vectors used in text.

[7] Y. Ueda and S. Okubo, Nucl. Phys. **49**, 345 (1963).

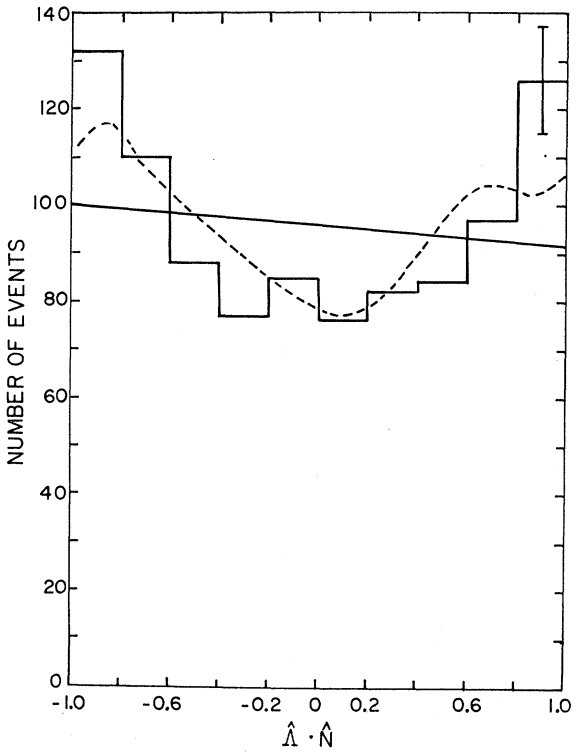


FIG. 7. The hisotgram presents the experimental data as a function of $\hat{\Lambda}\cdot\hat{N}$ for the zero-field events. The solid straight line is the expected distribution for our value of $\alpha P$ and no bias. The dashed curve is the distribution expected when the Monte-Carlo-calculated biases are taken into account.

The bias effects are most noticeable in the distribution of Eq. (2). Our data for the zero-field events are shown in Fig. 7, along with the straight line which would be expected for our value of $\alpha P$ and no bias; the loss of events near $\hat{\Lambda}\cdot\hat{N}=0$ is clearly evident. The dashed line is the distribution expected when the Monte-Carlo-calculated biases are taken into account.

The distribution of Eq. (3) was less severely distorted by bias effects.

According to the Monte Carlo calculation, the reasons for the observed biases are (in descending order of importance) as follows.

$(\hat{\Lambda}\cdot\hat{N})$: (1) The pion from the $\Xi^-$ decay stops in the spark-chamber walls; (2) the $\Lambda$ decays too far downstream to be detected by the spark chambers; (3) the pion from the $\Xi^-$ decay misses the downstream array of counters.

$(\hat{p}\cdot\hat{N})$: (1) $\Lambda$ hyperons whose decay proton is directed toward the beam line may not be detected because the decay pion and proton have a tendency to hit the same counter in the downstream array; (2) the pion from the $\Lambda$ decay stops in the spark-chamber walls.

From these studies we constructed, for each distribution, a one-parameter bias function $E(\theta)$. We investi-

gated $E(\theta)$ for the $\hat{\Lambda}\cdot\hat{N}$ and $\hat{p}\cdot\hat{N}$ distributions, assuming the decay parameters $\alpha=-0.4$, $\Phi=0$, $\alpha_\Lambda=0.646$, and various values of the $\Xi^-$ polarization $P$. We found that under these assumptions the polarization measurement should not be affected by our biases, provided no magnetic field was present. The decay-parameter measurements, however, were found to depend on the biases, and our results for these parameters depend to some extent on the accuracy of these calculations.

The effects of the magnetic field on detection efficiency were also studied, and bias functions for the two field directions and for the relevant distributions were deduced. The most useful distributions for the magnetic moment analysis are the two "projected-angle" intensity functions

$$2\pi I_\Lambda(\theta_\Lambda)=1+\tfrac{1}{4}\pi\alpha P\cos\theta_\Lambda, \quad (4)$$

$$2\pi I_p(\theta_p)=1+\tfrac{1}{12}\pi\alpha_\Lambda(2\gamma+1)P\cos\theta_p, \quad (5)$$

where the angles $\theta_\Lambda$ ($\theta_p$) are between the projections of $\boldsymbol{\Lambda}(\mathbf{p})$ and the polarization direction $\hat{N}$ on a plane normal to $\hat{\Xi}$ ($\hat{\Lambda}$). Use of these distributions rather than the space-angle distributions result in a slight loss in statistical accuracy but a large gain in simplification.

### B. Polarization and Decay Parameters

The calculations showed that the apparent polarization of the $\Xi^-$ sample would be affected by the presence of the magnetic field. Therefore $P$ was determined from the data with zero field, comprising 957 $\Xi^-$'s. The efficiency functions depend to some extent on the values of $\alpha$ and $\Phi$; the values used are consistent with the resulting values, and (in the case of $\alpha$) consistent with the previously known value.

Two essentially independent distribution functions give information on the polarization. One involves the parameter $\alpha$ and the other the parameters $\gamma$ and $\alpha_\Lambda$. One also finds independent information on the parameter $\alpha$ from the intensity function which depends on $\hat{p}\cdot\hat{\Lambda}$,

$$4\pi I_{p\Lambda}(\hat{p}\cdot\hat{\Lambda})=(1+\alpha\alpha_\Lambda\hat{p}\cdot\hat{\Lambda}), \quad (6)$$

which is independent of $P$. Thus this particular distribution may be used for analyzing the nonzero- as well as zero-field data.[8]

A maximum-likelihood analysis using the joint distribution function

$$I_{\Lambda N}(\hat{\Lambda}\cdot\hat{N})I_{p\Lambda}(\hat{p}\cdot\hat{\Lambda})$$

for the zero-field data and

$$I_{p\Lambda}(\hat{p}\cdot\hat{\Lambda})$$

for the nonzero-field data was carried out to find values for $P$ and $\alpha$. The effect of the calculated bias function $E(\theta)$ on the likelihood function is to introduce a normalization function which depends on the parameters. For example, $I_{\Lambda N}$ will be modified by a function $\eta_{\Lambda N}(\alpha,P)$ such that $\eta_{\Lambda N}\int E(\theta)(1+\alpha P\cos\theta)d\Omega=4\pi$. Details will be found in the thesis of one of the authors.[6] The likelihood function actually used for these distributions, which we will call method A, was

$$w=\sum_1^M \ln[(1+\alpha P\hat{\Lambda}_i\cdot\hat{N}_i)(1+\alpha\alpha_\Lambda\hat{\Lambda}_i\cdot\hat{p}_i)\eta_{\Lambda N}\eta_{\Lambda P}]$$
$$+\sum_1^{M'}\ln[(1+\alpha\alpha_\Lambda\hat{\Lambda}_i\cdot\hat{p}_i)\eta_{\Lambda P}],$$

where $M=957=$number of field-off events, and $M'=1476=$number of field-on events.

A separate analysis was made for $P$ and $\Phi$, with zero-field data only. Using the method described by Koch,[9] the distribution function for the angle

$$\psi=\tan^{-1}(\hat{p}\cdot\hat{Z}/\hat{p}\cdot\hat{Y})$$

can be found. It is

$$2\pi I_\psi(\psi)=1+(\tfrac{1}{4}\pi)^2\alpha_\Lambda P(\beta\cos\psi+\gamma\sin\psi). \quad (7)$$

A likelihood function was constructed as above, using only the $M$ field-off events and a normalization function $\eta_\psi$. To express $\beta$ and $\gamma$ in terms of $\Phi$, the $\alpha$ from method A was used. We will call this method B. Results from the two analyses are given in Table II. The information on $P$ from $\Lambda$ decay, method B, is nearly independent of the $\Xi^-$ decay information, method A, and we combine the two as independent to find $P=0.19\pm0.09$.

The disappointingly small value of $P$ led us to make a measurement, at the end of the experiment, in which the magnet was removed and spark chambers placed so that the $K^+$ direction could be measured, thus sharpening the production kinematics and the determination of $\hat{N}$. The result, with 164 $\Xi$'s, was $P=0.19\pm0.20$.

Our value of $P$, while much less than that indicated in earlier bubble-chamber work,[2] is only 1 standard deviation below that suggested by the recent compilation of Dauber *et al.*[10]

TABLE II. Results of the analysis for polarization and decay parameters of $\Xi^-$.

| | $P$ | $\alpha$ | $\Phi$ |
|---|---|---|---|
| This work, method A | $0.11\pm0.14$ | $-0.383\pm0.065$ | |
| This work, method B | $0.25\pm0.12$ | | $(-26\pm30)°$ |
| Dauber *et al.*, Ref. 10 | | $-0.39\ \pm0.04$ | $(-14\pm11)°$ |
| January 1969 compilation, Ref. 3 | | $-0.41\ \pm0.04$ | $(-3\pm9)°$ |

[8] The bias calculation shows that this is true even in the presence of bias effects.

[9] W. Koch, CERN Report No. 64-13 (unpublished).

[10] P. M. Dauber, J. P. Berge, J. R. Hubbard, D. W. Merrill, and R. A. Muller, Phys. Rev. **179**, 1262 (1969).

### C. Magnetic Moment

The primary purpose of this experiment was to measure the magnetic moment of the $\Xi^-$. However, the polarization of the sample proved to be only 2 standard deviations from zero, so that despite the nearly 1500 events and high magnetic field, the magnetic moment determination is only marginally meaningful.

Analysis of the data for the magnetic moment is greatly simplified by the fact that the vector $\hat{K}^-\times\hat{\Xi}^-$, and thus the initial spin axis, was nearly perpendicular to the magnetic field, and the trajectory of the $\Xi^-$ deviated from being parallel to **B** by only 9° on the average, 18° maximum. Thus the spin motion was, to a good approximation, a precession around **B**, the precession angle being given by

$$\theta_P=\frac{\mu e}{\beta\gamma M_p c^2}\int \mathbf{B}\cdot d\mathbf{l}\equiv\mu\Gamma, \tag{8}$$

where $\mu$ is the magnetic moment in units of $eh/2M_pc$, the nuclear magneton.[11] For a typical $\int\mathbf{B}\cdot d\mathbf{l}$ in our experiment, corresponding to $B=100$ kG, $\theta_P$ would be 9.6° for $\mu=1\ \mu_N$.

TABLE III. Results of the magnetic moment analysis, in nuclear magnetons.

| Magnetic moment | Projected-angle distribution | Field direction |
|---|---|---|
| $-4.8_{-1.8}^{+2.0}$ | $\Lambda$ | Upstream |
| $-4.8\pm4.6$ | $\Lambda$ | Downstream |
| $-4.8_{-1.8}^{+1.6}$ | $\Lambda$[a] | Combined |
| $2.0\pm1.6$ | Proton | Upstream |
| $-2.7_{-2.5}^{+3.0}$ | Proton | Downstream |
| $+1.2_{-1.6}^{+1.5}$ | Proton[a] | Combined |
| $-0.1\pm2.1$ | Combined[a] | Combined |

[a] It should be noted that the error of the combined result is larger than the individual errors from either the proton or $\Lambda$ projected-angle distribution. This results from the correct likelihood analysis as discussed in the text (see Sec. IV C).

We have used the projected-angle distribution, Eqs. (4) and (5), modified by the (assumed) spin rotation and the appropriate bias functions to form the likelihood function for magnetic moment analysis.

These two distributions have quite different bias effects, as shown in Figs. 8(a) and 8(b), so it is a measure of consistency to intercompare them. For the actual values of the $\Xi^-$ decay parameters, the two are nearly statistically independent (this can be seen, for instance, by comparing the results for $P$ from the joint distribution function with the results from the two distributions, combined as though independent). We therefore found separate maximum-likelihood solutions for each distribution, and for each of the two field directions.

An apparent spin rotation, and therefore a spurious value for the magnetic moment, can be introduced by a detection asymmetry which has a screw sense (e.g., two successive azimuthal asymmetries). Any such asymmetry which is not field dependent will cancel out when the sample consists of equal numbers of field-parallel and field-antiparallel events. We thus expect that even without the efficiency calculations there is a first-order cancellation of spurious effects. The efficiency calculations, which agreed well with the field-off data, included all field-dependent effects we could find. The only significant one was an enhanced absorption of the $\pi^-$ from $\Xi^-$ in the spark-chamber wall when the field bent the $\pi^-$ away from the axis; the effect of this proved to be small compared with the statistical error.

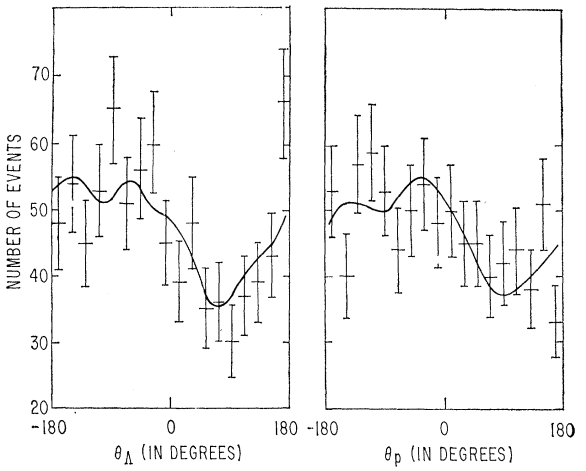


FIG. 8. Experimental data as a function of the projected angles (a) $\theta_\Lambda$ and (b) $\theta_p$ (see Sec. IV B for definition of $\theta_\Lambda$ and $\theta_p$). The solid curve is the expected distribution as derived from the Monte Carlo calculation using our values for $\alpha P$ and $\mu_\Xi$, and employing the appropriate bias correction.

The four likelihood functions had the form

$$w=\sum_1^{M'}\ln\{[1+AP\cos(\chi_j+\mu\Gamma_j)]\eta\}, \tag{9}$$

where $\chi_j$ is the appropriate projected angle and $\Gamma_j$ is the magnetic field parameter [see Eq. (8)] for the $j$th event; $A$ is the appropriate asymmetry parameter, with polarization $P$ constrained to have the value found in the no-field data[12]; $\eta$ is the normalization function, and $\mu$ is the magnetic moment in nuclear magnetons. The results of maximizing these are shown in Table III. Likelihood curves for the $\Lambda$- and $p$-projected distributions (field directions combined) are given in Fig. 9.

The results for the two field directions are seen to be reasonably consistent. Also, the result combining all four distributions, $\mu=-(0.1\pm2.1)\ \mu_N$, is consistent with the combined result we obtained with *no efficiency function* included, $\mu=-(0.8\pm1.8)\mu_N$. However, the $\Lambda$-

[11] The small corrections to this approximation are studied by Sander (Ref. 4).

[12] The value of $P$ found from these distributions was actually 0.13, intermediate between the two values of Table II.

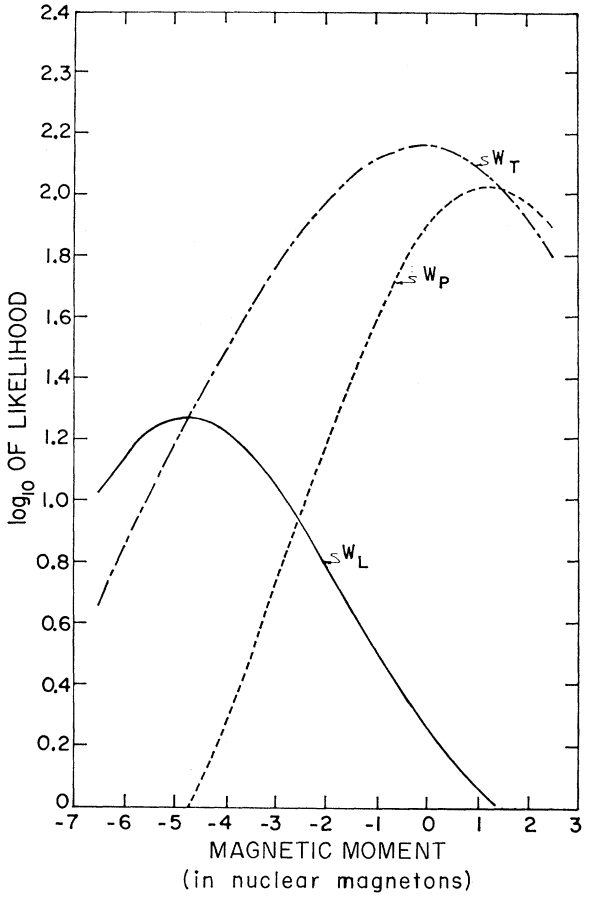


FIG. 9. Likelihood versus the value of the magnetic moment. Solid curve, labeled $W_L$, is obtained from the distribution in $\theta_\Lambda$ involving the $\Lambda$ momentum. The dashed curve, labeled $W_T$, is derived from the joint distribution in $\theta_p$ and $\theta_\Lambda$. Both signs of magnetic field are included in all curves.

and $p$-projected-angle distributions disagree by an amount larger than one would expect. The $\chi^2$ of the four results in Table III, if the true value is $-0.1\ \mu_N$, has a probability of 0.02. (It will be noted that the "combined" values in Table III are not directly related to the quoted errors, which are simply half-widths at $w=w_{\max}-0.5$; they are obtained by adding likelihoods, so that the $\Lambda$ distribution, which has a non-Gaussian likelihood curve, gets less weight than the $p$ distribution.) We have not been able to account for this apparent lack of consistency, but we note that the statistical method used, combination of likelihoods, automatically gives a value for the error which takes the inconsistency into account.

## V. CONCLUDING REMARKS

The value found for the magnetic moment, $-(0.1\pm2.1)\ \mu_N$, is scarcely more than an indication that the moment can be measured, and that it is probably not large. It will be recalled that the $SU_3$ prediction[13] is $-(\mu_p+\mu_n)=-0.9\mu_N$.

The value for the asymmetry decay parameter, $\alpha=-0.383\pm0.065$, will lower slightly the world-average value of $-0.41\pm0.04$. The value for $\Phi$, $(-26\pm30)°$, has a considerably larger error than the world average, $(-3\pm9)°$, so it serves only to confirm that $\gamma=(1-\alpha^2)^{1/2}\times\cos\Phi$ is positive, that is, $S$ wave predominates in the $\Xi^-$ decay.

In general, our expectations that the $\Xi^-$ would be well suited to spark-chamber measurements of the decay parameters and magnetic moment were confirmed. Better information on $\Phi$ and the magnetic moment will await the discovery of production conditions under which the $\Xi^-$ has a large polarization.

## ACKNOWLEDGMENTS

It is a pleasure to acknowledge the invaluable assistance of Frederick Toevs, James Schultz, Bruce Brown, Lee Knapp, and Peter Garrow. We thank Dr. E. J. Lofgren and W. D. Hartsough and the staff at the Bevatron for their hospitality and assistance throughout the data-taking phase of the experiment.

[13] S. Coleman and S. L. Glashow, Phys. Rev. Letters 6, 423 (1961).

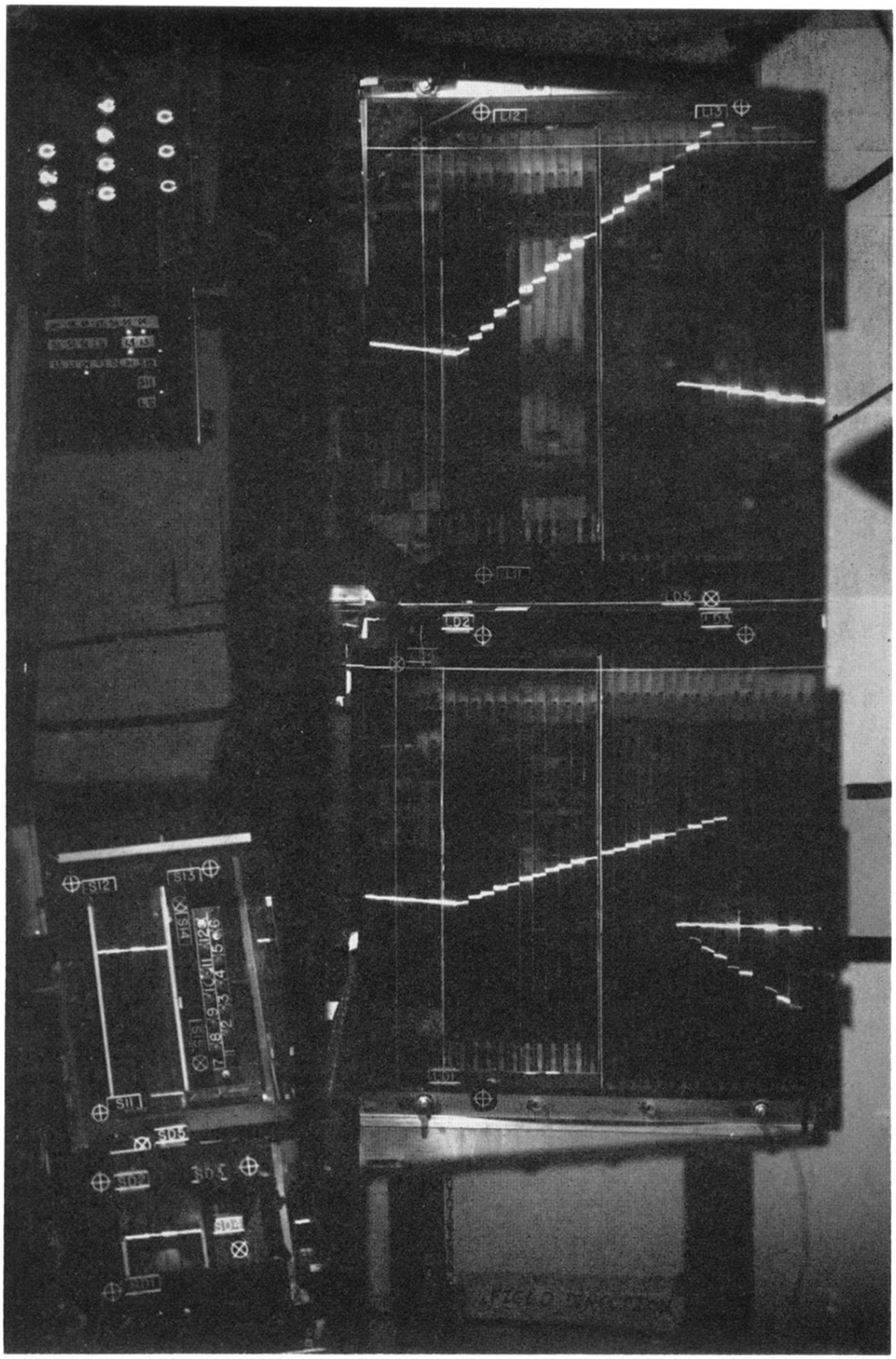

FIG. 3. Example of cascade decay event seen in spark chambers SC3, SC4, and SC5. Cascade enters from left and decays into $\pi^-$ and $\Lambda^0$. Subsequent decay of $\Lambda^0$ into $p+\pi^-$ is seen in far right of chambers.